scientific reports

Check for updates

OPEN

Haemodynamic study of left nonthrombotic iliac vein lesions: a preliminary report

Yun Pei[1,2], Qijia Liu[1,2] & Xuan Li[1]✉

Nonthrombotic iliac vein lesions (NIVLs) are significant causes of chronic venous insufficiency (CVI) in the left lower limb and symptom recurrence following left lower limb varicose vein treatment. The goal of this study was to explore the haemodynamic and morphological characteristics of iliac veins in patients with NIVLs. Pressure at the caudal end of the stenotic left common iliac vein (LCIV) segment, local blood flow velocity, and time-averaged wall shear stress in the stenotic segment exhibited positive correlations with the clinical CVI classification (R = 0.92, $p < 0.001$; R = 0.94, $p < 0.001$; R = 0.87, $p < 0.001$), while the relative retention time showed a negative correlation (R = -0.94, $p < 0.001$). The pressure difference (ΔP) between the two ends of the stenotic segment and the velocity difference (ΔV) between the stenotic segment and the caudal end were positively correlated with the clinical classification (R = 0.92, $p < 0.001$; R = 0.9, $p < 0.001$). The cross-sectional area stenosis rate and length of the stenotic LCIV segment were positively correlated with the clinical classification (R = 0.93, $p < 0.001$; R = 0.63, $p < 0.001$). The results suggest that haemodynamic assessment of the iliac vein could effectively portray blood flow disturbances in stenotic segments of the LCIV, potentially reflecting the degree of iliac vein stenosis. Haemodynamic indicators are correlated with the severity of clinical CVI symptoms.

Keywords Nonthrombotic iliac vein lesions, Chronic venous insufficiency, Haemodynamics, Morphology, Computer simulation

Nonthrombotic left iliac vein lesions (NIVLs) typically occur when the left common iliac vein (LCIV) and/or inferior vena cava (IVC) are compressed by the right common iliac artery and the fifth lumbar vertebra[1]. Venous hypertension caused by NIVLs is an aetiological factor of chronic venous insufficiency (CVI) in the left lower limb, playing a permissive role in its pathogenesis; NIVLs are also a significant cause of symptom recurrence after treatment for left lower limb varicose veins, yet they are often overlooked clinically[1–4]. Given the importance of this condition, endovascular treatment has emerged as a promising approach to alleviate CVI symptoms associated with NIVLs in the left lower limb and has garnered increased clinical attention[5]. However, the lack of effective, objective assessment methods has resulted in controversies in determining suitable clinical indications[5].

This study employed computational fluid dynamics (CFD) to perform haemodynamic simulations for analysing the haemodynamic and morphological characteristics of the left iliac vein and IVC. By examining the correlations between various haemodynamic alterations and the severity of clinical symptoms (clinical classification) in NIVL patients, this study aimed to provide objective evidence for the diagnosis and treatment of NIVLs.

Results

Medical records

A total of 24 subjects, comprising 7 males and 17 females, with ages ranging from 17 to 71 years, were included in this study. Groupings based on the clinical classification are s shown in Table 1.

Haemodynamic indicators (Table 2)

The pressure at the caudal end of the stenotic LCIV segment increased with increasing clinical classification, whereas the pressure at the cranial end of the stenosis segment decreased, occasionally below the pressure in the lower segment of the IVC (Fig. 1). Specifically, the pressure at the caudal end of the stenotic LCIV segment (P1) exhibited a significant positive correlation with the clinical classification (R = 0.92, $p < 0.001$; Fig. 2A). Intergroup

[1]Department of Interventional Radiology and Vascular Surgery, Peking University Third Hospital, 49 North Huayuan Road, Haidian District 100191, Beijing, China. [2]These authors contributed equally: Yun Pei and Qijia Liu. ✉email: xuanli@vip.sina.com

Groups	Clinical classifications	Male	Female	Age*
A ($n=8$)	C_{0a}	2	6	53.33 ± 9.87 (38–65)
B ($n=8$)	C_{0s} and C_{1-2}	3	5	61.17 ± 7.02 (52–71)
C ($n=8$)	C_{3-6}	2	6	49.89 ± 15.37 (17–68)

Table 1. Basic Data and Grouping of Included Subjects in this Study. *Age is expressed as mean ± standard deviation (minimum–maximum).

Hydrodynamic indicators	A ($n=8$)	B ($n=8$)	C ($n=8$)	Experimental group ($n=16$)	*p*-value*	*p*-value#	*p*-value†	*p*-value‡
P1 (Pa)	1300 (162)	1968 (458)	4677 (1347)	3222 (1703)	0.003	0.261	< 0.001	< 0.001
P2 (Pa)	1011 (177)	1059 (475)	512 (584)	786 (587)	0.304	0.975	0.088	0.058
ΔP (Pa)	289 (126)	909 (417)	4165 (1610)	2537 (2029)	0.005	0.418	< 0.001	< 0.001
V1 (m/s)	1.03 (0.35)	1.72 (0.35)	3.01 (0.60)	2.366 (0.82)	< 0.001	0.016	< 0.001	< 0.001
V2 (m/s)	0.78 (0.25)	1.13 (0.25)	0.76 (0.30)	0.94 (0.33)	0.238	0.042	0.979	0.028
ΔV (m/s)	0.25 (0.15)	0.59 (0.24)	2.26 (0.49)	1.42 (0.94)	0.002	0.119	< 0.001	< 0.001
TAWSS (Pa)	1.26 (0.58)	2.00 (0.59)	6.53 (2.11)	4.27 (2.78)	0.007	0.504	< 0.001	< 0.001
RRT (s)	1.76 (0.96)	0.47 (0.19)	0.14 (0.03)	0.31 (0.21)	< 0.001	< 0.001	< 0.001	0.491

Table 2. Values of hemodynamic indicators. Values are presented as mean (standard deviation). P1 = Pressure at the caudal end of the stenotic segment of the left common iliac vein (LCIV); P2 = Pressure at the cranial end of the stenotic segment of LCIV; ΔP = P1–P2; V1 = Blood flow velocity in the stenotic segment of LCIV; V2 = Blood flow velocity at the confluence of the left internal and external iliac vein; ΔV = V1–V2; TAWSS = Time-averaged wall shear stress in the stenotic segment of LCIV; RRT = Relative residence time in the stenotic segment of LCIV. A = Control group (C_{0a}); B = Mild group (C_{0s} and C_{1-2}); C = Moderate to severe group (C_{3-6}). *Comparison of mean value changes between the control group (Group A) and the experimental groups (Groups B and C); #Comparison of mean value changes between Group A and Group B; †Comparison of mean value changes between Group A and Group C; ‡Comparison of mean value changes between Group B and Group C.

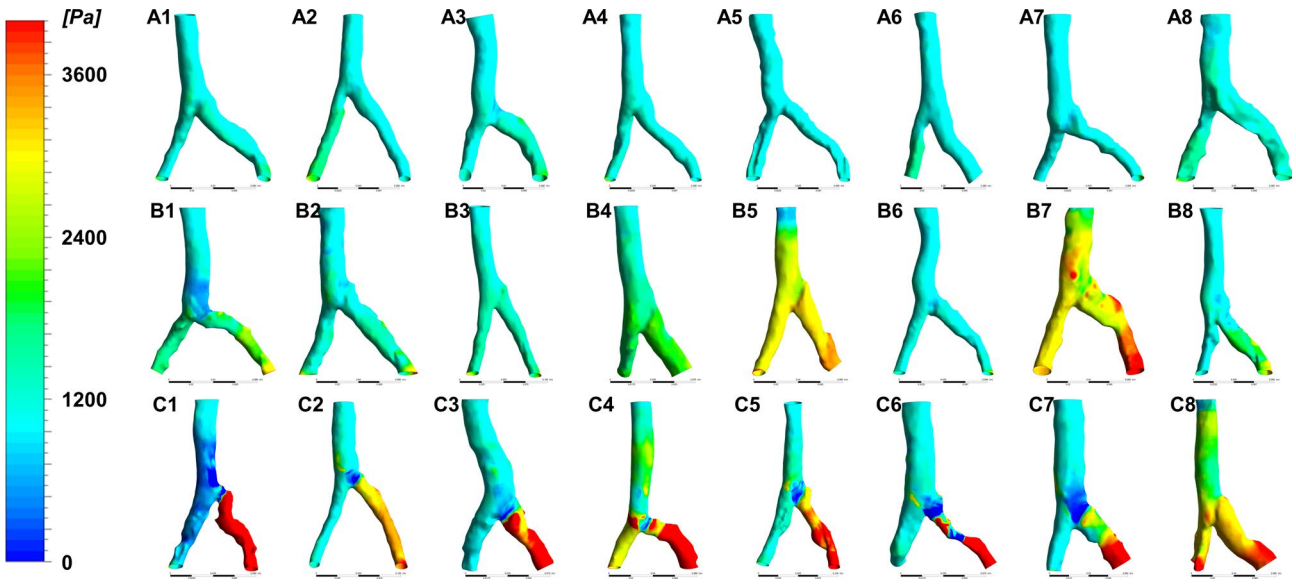

Figure 1. Pressure of the bilateral iliac veins and inferior vena cava (IVC) in 24 subjects. The pressure at the caudal end of the stenotic segment of the left common iliac vein (LCIV) gradually increases with increasing clinical classification, with the most substantial increase observed in Group C subjects (red area). Conversely, the pressure at the cranial end of the stenotic segment of the LCIV significantly decreases, even dropping below the pressure level at the IVC (blue area), with increasing clinical classification. A1-A8: Group A, control group (C_{0a}); B1-B8: Group B, mild group (C_{0s} and C_{1-2}); C1-C8: Group C, moderate to severe group (C_{3-6}).

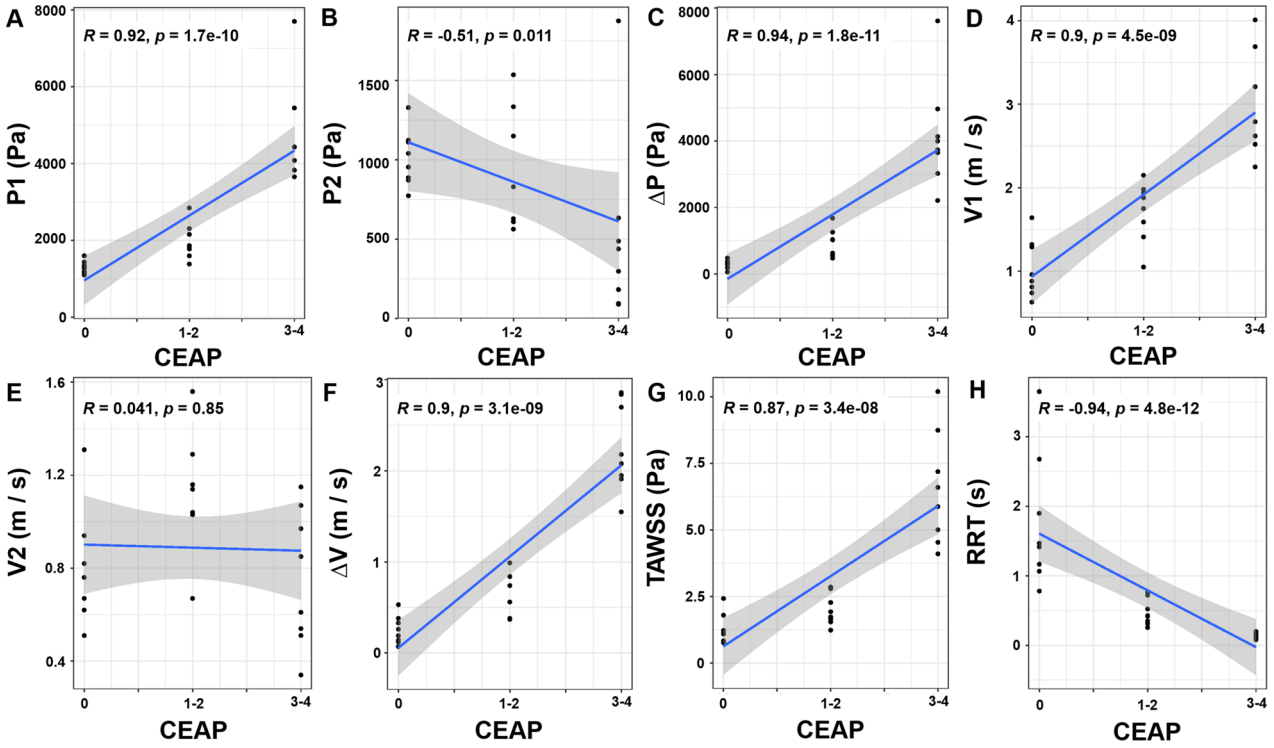

Figure 2. Analysis of the correlations between haemodynamic indicators and clinical classification. (**A**) Pressure at the caudal end of the stenotic segment of the left common iliac vein (LCIV) (P1); (**B**) Pressure at the cranial end of the stenotic LCIV segment (P2); (**C**) Pressure difference between the two ends of the stenotic LCIV segment (ΔP, ΔP = P1–P2); (**D**) Blood flow velocity in the stenotic LCIV segment (V1); (**E**) Blood flow velocity at the confluence of the left internal and external iliac vein (V2); (**F**) Blood flow velocity difference between the stenotic segment of the LCIV and the caudal end (ΔV, ΔV = V1–V2); (**G**) Time-averaged wall shear stress (TAWSS) in the stenotic LCIV segment; (**H**) Relative residence time (RRT) in the stenotic LCIV segment. (**A**) Control group (C_{0a}); (**B**) Mild group (C_{0s} and $C_{1\text{-}2}$); (**C**) Moderate to severe group ($C_{3\text{-}6}$). For each group, $n = 8$.

comparisons of P1 revealed significant differences between the experimental group and the control group as well as between Group C and Groups A and B. However, no significant difference was observed between Groups B and A. Conversely, the pressure at the cranial end of the stenotic LCIV segment (P2) displayed a significant negative correlation with the clinical classification (R = -0.51, $p = 0.011$; Fig. 2B). However, there were no significant differences in P2 among the groups. The difference between P1 and P2 (ΔP) represents the pressure difference at the two ends of the stenotic LCIV segment, which was significantly positively correlated with clinical classification (R = 0.94, $p < 0.001$; Fig. 2C). Intergroup comparisons of ΔP indicated significant differences between the experimental group and the control group and between Group C and Groups A and B. Furthermore, although the ΔP of Group B exceeded that of Group A, the difference was not significant. According to the optimization function, the threshold value of ΔP between Groups A and B was 433.2 Pa, and that between Groups B and C was 1578.6 Pa.

The blood flow velocity within the stenotic LCIV segment increased with the clinical classification, showing a positive correlation (Supplementary Fig. S1). Specifically, the blood flow velocity in the stenotic LCIV segment (V1) was significantly positively correlated with the clinical classification (R = 0.9, $p < 0.001$; Fig. 2D). Statistically significant differences in V1 were observed among the groups; in contrast, the blood flow velocity at the confluence of the left internal and external iliac veins (V2) remained consistent across all groups and was not related with the clinical classification (R = 0.041, $p = 0.95$; Fig. 2E). The difference between V1 and V2 (ΔV), representing the difference in blood flow velocity between the stenotic segment of the LCIV and the caudal end, exhibited a significant positive correlation with the clinical classification (R = 0.9, $p < 0.001$; Fig. 2F). Intergroup comparisons of ΔV revealed significant differences between the experimental group and the control group and between Group C and Groups A and B. While the ΔV of Group B exceeded that of Group A, the difference was not considered significant. According to the optimization function, the threshold value of ΔV between Groups A and B was 0.5 m/s, and that between Groups B and C was 1.1 m/s.

The time-averaged wall shear stress (TAWSS) within the stenotic LCIV segment exhibited a notable increase, while the TAWSS at either end of the stenotic segment markedly decreased (Supplementary Fig. S2). Specifically, the TAWSS in the stenotic LCIV segment was significantly positively correlated with the clinical classification (R = 0.87, $p < 0.001$; Fig. 2G). Significant differences in the TAWSS were observed between the experimental group and the control group and between Group C and Groups A and B. Although the TAWSS within the stenotic segment of Group B surpassed that of Group A, the difference was not considered significant.

The relative residence time (RRT) within the stenotic LCIV segment was notably shorter than that at both ends of the stenosis segment within the vein (Supplementary Fig. S3). Specifically, the RRT of the stenotic LCIV segment exhibited a significant negative correlation with the clinical classification ($R = -0.94$, $p < 0.001$; Fig. 2H). Intergroup comparisons indicated a significant difference in the stenosis segment RRT between the experimental group and the control group. Although the RRT of Group C was shorter than that of Group B, the difference was not considered significant.

Morphological indicators (Table 3)

Both S1 and S2 exhibited significant negative correlations with the clinical classification ($R = -0.83$, $p < 0.001$; $R = -0.55$, $p = 0.006$; Fig. 3A,B). Significant differences in S1 were observed among the groups, whereas there were no significant differences in S2. The cross-sectional area stenosis rate of the stenotic LCIV segment demonstrated a significantly positive correlation with the clinical classification ($R = 0.93$, $p < 0.001$; Fig. 3C). Significant differences in the cross-sectional area stenosis rate were observed among the groups. According to the optimization function, the threshold value of the cross-sectional area stenosis rate between Groups A and B was 24.3%, and that between Groups B and C was 44.2%. S3 was not correlated with the clinical classification, and it was not significantly different among the groups ($R = -0.2$, $p = 0.35$; Fig. 3D). However, the S1/S3 ratio showed a significant negative correlation with the clinical classification ($R = -0.92$, $p < 0.001$; Fig. 3E), with significant differences observed among the groups. θ in each group remained consistent and did not demonstrate a linear relationship with the clinical classification ($R = 0.2$, $p = 0.35$; Fig. 3F). Additionally, there were no significant differences in θ between the groups. L1 was significantly positively correlated with the clinical classification ($R = 0.63$, $p < 0.001$; Fig. 3G). Intergroup comparisons revealed significant differences in L1 between the experimental group and the control group and between Group C and Group A. Although L1 in Group B was larger than that in Group A and smaller than that in Group C, the differences were not significant. L2 was similar among the groups and did not exhibit a linear relationship with the clinical classification ($R = 0.35$, $p = 0.097$; Fig. 3H).

Discussion

Lower extremity CVI is a prevalent condition in vascular surgery, with stenosis or obstruction of the iliac vein and/or inferior vena cava frequently significant contributors to its onset[2,3,6]. The American Venous Forum proposed the CEAP classification in 1993, which was subsequently revised in 2020, based on the clinical manifestations (C), aetiology (E), anatomy (A), and pathophysiology (P) of patients with lower extremity CVI[7]. Notably, the clinical classification is highly important in assessing CVI[7,8]. Within the CEAP classification, C_0 corresponds to patients devoid of visible or palpable signs of venous disease and thus are frequently overlooked by clinicians. Further subdivision of C_0 includes those without lower limb symptoms (C_{0a}) and those presenting with symptoms (C_{0s})[7]. Currently, there is still controversy surrounding the selection of patients for endovascular treatment of NIVLs. Most scholars agree that patients with moderate to severe symptoms and those unresponsive to conservative treatment may opt for endovascular therapy. Therefore, in this study, nonvascular disease patients (C_{0a}) composed the control group, while patients exhibiting lower extremity CVI ($C_{0s\text{-}6}$) composed the experimental group, further subdivided based on the severity of clinical symptoms. Haemodynamic simulation, a noninvasive method, is then employed to analyse the local haemodynamic and morphological characteristics of the iliac and inferior vena cava veins, assessing the impact of NIVLs on iliac vein haemodynamics[9]. Although intravascular

Morphological indicators	A ($n = 8$)	B ($n = 8$)	C ($n = 8$)	Experimental group ($n = 16$)	p-value*	p-value#	p-value†	p-value‡
S1 (mm^2)	191.5 (36.1)	139.3 (43.8)	72.4 (29.1)	105.8 (48.8)	< 0.001	0.026	< 0.001	0.004
S2 (mm^2)	228.1 (41.6)	211.6 (62.6)	169 (47.1)	190.3 (57.9)	0.115	0.798	0.077	0.242
Cross-sectional area stenosis rate (%)	15.8 (6.9)	34.2 (8.1)	58.4 (11.5)	46.3 (15.7)	< 0.001	< 0.001	< 0.001	< 0.001
S3 (mm^2)	379.6 (66.8)	358.5 (99.7)	334.3 (88.8)	346.4 (92.1)	0.375	0.877	0.553	0.841
S1/S3 (%)	50.8 (8.2)	38.9 (4.6)	22.5 (9.5)	30.7 (11.1)	< 0.001	0.014	< 0.001	0.001
θ(°)	61.7 (15.2)	63.9 (25)	69.3 (18.3)	66.6 (21.4)	0.570	0.973	0.73	0.853
L1 (mm)	5.3 (1.5)	7.4 (1.8)	11 (5.4)	9.2 (4.3)	0.023	0.46	0.008	0.106
L2 (mm)	16.3 (7.3)	13.2 (2.6)	24.25 (13.9)	18.7 (11.2)	0.582	0.786	0.216	0.064

Table 3. Values of morphological indicators. Values are presented as mean (standard deviation). S1 = Minimum cross-sectional area of the left common iliac vein (LCIV) stenotic segment; S2 = Cross-sectional area of the caudal end of the LCIV stenotic segment; Cross-sectional area stenosis rate = (1–S1/S2) × 100%; S3 = Cross-sectional area of the confluence of the bilateral common iliac veins; θ = Bifurcation angle at the confluence of the centerlines of the bilateral common iliac veins; L1 = Length of the LCIV stenotic segment; L2 = Distance from the narrowest point of LCIV to the confluence point of the centerlines of the bilateral common iliac veins. A = Control group (C_{0a}); B = Mild group (C_{0s} and $C_{1\text{-}2}$); C = Moderate to severe group ($C_{3\text{-}6}$). *Comparison of mean value changes between the control group (Group A) and the experimental groups (Groups B and C); #Comparison of mean value changes between Group A and Group B; †Comparison of mean value changes between Group A and Group C; ‡Comparison of mean value changes between Group B and Group C.

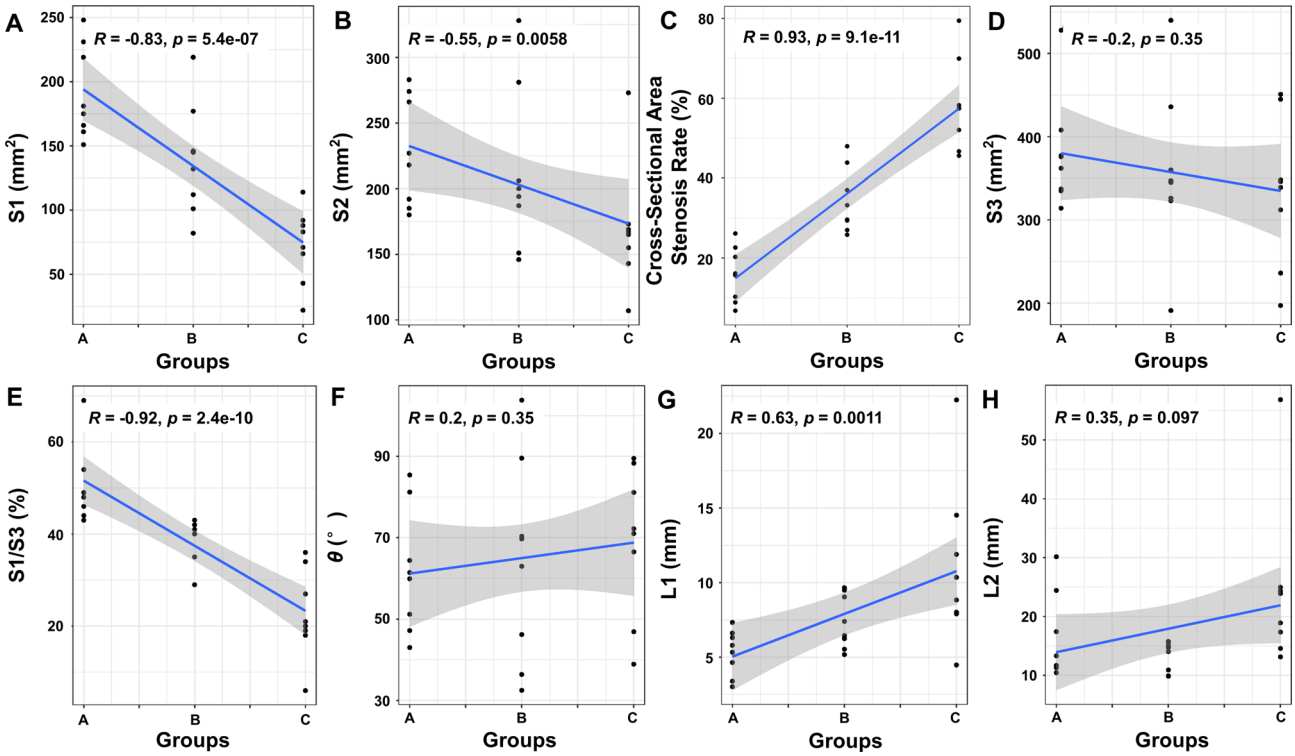

Figure 3. Analysis of the correlations between morphological indicators and clinical classification. (**A**) Minimum cross-sectional area of the stenotic segment of the left common iliac vein (LCIV) (S1); (**B**) Cross-sectional area of the caudal end of the stenotic LCIV segment (S2); (**C**) Cross-sectional area stenosis rate = (1–S1/S2) × 100%; (**D**) Cross-sectional area of the confluence of the bilateral common iliac veins (S3); E: Ratio of S1 to S3; F: Bifurcation angle at the confluence of the centrelines of the bilateral common iliac veins (θ); (**G**) Length of the stenotic LCIV segment (L1); (**H**) Distance from the narrowest point of the LCIV to the confluence point of the centrelines of the bilateral common iliac veins (L2). (**A**) Control group (C_{0a}); (**B**) Mild group (C_{0s} and $C_{1\text{-}2}$); (**C**) Moderate to severe group ($C_{3\text{-}6}$). For each group, $n = 8$.

ultrasound is currently an important diagnostic and therapeutic tool, it is undeniably an invasive procedure, whereas the noninvasive nature of haemodynamic simulation offers distinct advantages[9].

Haemodynamic simulation is a pivotal tool for revealing the intricacies of blood flow within the circulatory system. In recent years, a large number of studies have conducted research on haemodynamic simulations, with a plethora of sophisticated haemodynamic models emerging to accurately replicate various blood flow phenomena within the human body[10–13]. These models offer invaluable assistance in the diagnosis and treatment of cardiovascular diseases. The advent of individualized modelling, leveraging imaging data to construct precise three-dimensional (3D) models of vascular systems, has revolutionized haemodynamic research[14–16]. By observing haemodynamic alterations at the local and systemic levels, individualized modelling enables a comprehensive understanding of disease pathogenesis, progression, and treatment efficacy. CFD, a cornerstone in haemodynamic simulation, is widely employed in the construction of human vascular models and subsequent haemodynamic investigations[14,17]. In this study, CFD was used to simulate the local haemodynamics of left NVILs, allowing an assessment of its impact on changes in lower extremity CVI symptoms.

The findings of this study indicated a significant increase in pressure at the caudal end of the stenotic LCIV segment, accompanied by increased blood flow velocity, greater TAWSS, and shorter RRT within the stenotic segment, aligning closely with those of a previous report[18]. Moreover, the results of this study revealed a correlation between these haemodynamic changes and the severity of the clinical symptoms of CVI. The substantial pressure difference at both ends of the stenotic LCIV segment may induce severe haemodynamic disturbances, potentially resulting in local venous vessel wall damage, exacerbating venous stenosis, and precipitating venous hypertension at the caudal end of the stenotic segment. Such effects could contribute to the progression of lower extremity CVI and potentially predispose the individual to lower extremity deep vein thrombosis[2,9,18,19]. Notably, this study also revealed a decrease in pressure at the cranial end of the stenotic LCIV segment, occasionally dropping below the pressure within the IVC. This phenomenon could be attributed to the Bernoulli effect in fluid dynamics. Given the nonslip rigid wall setting of the vascular wall in this study, adherence to the Bernoulli principle was ensured.

In this study, ΔP and ΔV were significantly correlated with the clinical classification, underscoring their potential as objective indicators for guiding clinical surgery. Substantial differences in ΔP and ΔV were observed between the experimental group and the control group, as well as between the moderate to severe group ($C_{3\text{-}6}$) and the mild group ($C_{0s\text{-}2}$). Conversely, the differences between the mild group and the control group (C_{0a}) were not significant. These findings suggest that ΔP and ΔV may serve as indirect indicators of the degree of LCIV stenosis, offering valuable guidance for clinical decision-making. Notably, advances in vascular ultrasound

technology have made it possible to accurately measure blood flow velocity and offered hope that vascular pressure can also be evaluated through vascular ultrasound examination in the foreseeable future[20]. The eventual accessibility of both the ΔP and ΔV through noninvasive means could significantly improve clinical practice, allowing improved patient care and treatment strategies.

The unique local anatomy of the left iliac vein results in distinct challenges, including compression by the right iliac artery and lumbar vertebral bodies and the potential formation of fibrous bands within stenotic vein segments[17]. Consequently, the cross-sectional area of the stenotic segment often assumes an irregular shape. Traditional methods, such as calculating the stenosis rate based on vessel diameter, may inadequately reflect the impact of vascular lesions on haemodynamics. Therefore, in this study, 3D modelling of the iliac vein allowed the use of the cross-sectional area to calculate the stenosis rate, which served as an evaluation index. This approach effectively circumvents errors stemming from irregular cross-sectional areas of venous vessels. Presently, most imaging devices support automatic measurement of vessel cross-sectional area, which could reduce the impact of human measurement errors when utilizing the cross-sectional area stenosis rate as a diagnostic criterion. A previous study indicated a high incidence of NVILs in asymptomatic individuals; approximately 66% of population had an LCIV compression stenosis rate exceeding 25%, with an overall average of 35.5%[21]. Consistent with these findings, in this study, varying degrees of compression stenosis were identified in the LCIV of asymptomatic subjects within the control group, with a cross-sectional area stenosis rate of 15.8% ± 6.9%. Discrepancies in the stenosis rate may have arisen from differences in the calculation methods, which could also account for the absence of clinically relevant symptoms in the LCIV stenosis population. Moreover, this study revealed a significant correlation between the cross-sectional area stenosis rate of the stenotic LCIV segment and the clinical classification. Distinct thresholds were observed between the control group and the mild group and between the mild group and the moderate to severe group (24.3% and 44.2%, respectively). These findings suggest that the cross-sectional area stenosis rate of the stenotic LCIV segment quantitatively corresponds with the severity of symptoms in patients with lower extremity CVI, offering another promising, objective indicator for guiding treatment decisions.

Several scholars have suggested that the confluence angle of the bilateral iliac vein could impact the wall shear stress within the stenotic iliac vein segment and the pressure difference around it[18,19]. Similarly, our investigation revealed a potential correlation between the confluence angle of the bilateral iliac vein and the clinical classification. However, statistical analysis revealed no significant differences, which might be attributed to the selection and grouping of the study subjects as well as the relatively small sample size in this study.

Moreover, our study revealed a positive correlation between the length of the stenotic LCIV segment and the clinical classification, in line with fluid physics principles. This suggests that as the length of the stenotic LCIV segment increases, so does the severity of blood flow disturbance, while the shear and friction forces on the vascular wall also increase. Consequently, this leads to more profound vascular damage and elevated vascular pressure. Hence, standardized measurement of the length of the stenotic LCIV segment could serve as a crucial factor in the treatment decision-making process for NVIL patients.

Importantly, while CFD based on mathematical models offers valuable insights, it is inherently limited in the ability to fully replicate the intricate haemodynamics and pathological variability of the cardiovascular system. Unlike those of the arterial vessels, venous vessel walls are thin and flexible and are influenced by respiratory movements, thus increasing the complexity of modelling efforts. Therefore, the outcomes derived from CFD should be regarded as references rather than exact replicas of physiological processes. Due to stringent inclusion criteria and the stratification of subjects based on clinical classification of CVI, subjects in the moderate to severe group were relatively scarce, resulting in only 24 subjects being included in this study. Nonetheless, rigorous numerical simulations have clearly demonstrated the significance of CFD in assessing left NIVLs. Moreover, the collateral circulation of the iliac veins in NIVL patients exhibits considerable diversity and complexity, varying significantly among patients. Due to sample size limitations, this study did not conduct subset analysis of collateral circulation. Currently, artificial intelligence technology is advancing rapidly. We anticipate that artificial intelligence will soon integrate seamlessly with 3D vascular model construction and haemodynamic simulation, alleviating the burden of human modelling. The more precise models, algorithms, and larger-scale studies can provide more accurate clinical information for the diagnosis and treatment of NVILs.

In conclusion, haemodynamic analysis provided crucial insights into the haemodynamic changes occurring within the stenotic segment of the LCIV and its surrounding vasculature. These changes include venous hypertension at the caudal end of the stenotic LCIV segment, high blood flow velocity, an elevated TAWSS, and reduced RRT within the stenosis segment, all of which are indicative of lower extremity CVI progression. Moreover, indicators such as the ΔP, ΔV, and cross-sectional area stenosis rate exhibited positive correlations with the clinical classification, serving as direct or indirect indicators of the severity of LCIV stenosis. Additionally, the length of the stenotic segment correlated positively with the clinical classification. These objective, quantitative measures provide valuable means for assessing the severity of the condition of patients with NIVLs, aiding clinical diagnosis and optimizing treatment planning.

Methods

Medical records

Approval for this retrospective study from Peking University Third Hospital Medical Science Research Ethics Committee (Ethics Approval: 2023-675-01). This study was conducted in accordance with the Helsinki Declaration.

Subject inclusion criteria

(a) Control Group: No vascular disease or symptoms of lower limb CVI and previous enhanced abdominal-pelvic computed tomography (CT) examination.
(b) Experimental Group: Isolated left lower limb CVI and evident compression stenosis of the LCIV, as shown on enhanced abdominal-pelvic CT.

Subject exclusion criteria

(a) CVI in both lower limbs.
(b) Isolated left lower limb CVI and no prior enhanced abdominal-pelvic CT examination.
(c) Isolated left lower limb CVI lacking evident compression stenosis of the LCIV, as shown on enhanced abdominal-pelvic CT.
(d) Left lower limb CVI and venous thrombosis.

Grouping

A total of twenty-four subjects participated in this study, with 8 in the control group and 16 in the experimental group. All subjects underwent abdominal-pelvic enhanced CT scans, and lower limb vascular ultrasound ruled out venous thrombosis in the left lower limb. The subjects were categorized into 3 groups based on the clinical (C) classification of CVI[7]: Group A: control group (C_{0a}); Group B: mild group (C_{0s} and $C_{1\text{-}2}$); and Group C: moderate to severe group ($C_{3\text{-}6}$).

Three-dimensional model construction

CT was performed utilising a 64-slice multidetector scanner (LightSpeed VCT; GE HealthCare), with 0.625 mm slice thickness. The original DICOM-format CT images were imported into Mimics software (Materialise) to generate masks delineating the IVC and bilateral common iliac veins. This process involved utilizing algorithms such as threshold segmentation, region growing, and manual editing. Subsequently, postprocessing refinement was conducted in 3-Matic Medical (Materialise) to produce smooth 3D models, including smoothing, surface fitting, and artefact removal. The vascular centrelines for the IVC-LCIV and IVC-right common iliac vein (RCIV) were then derived. Next, the inlet and outlet perpendicular to the vascular centrelines were established. The inlet was positioned at the confluence of the bilateral internal iliac vein and external iliac vein, while the outlet was set one centimetre below the lower margin of the left renal vein.

Haemodynamic analysis

Following mesh optimization within 3-Matic Medical, volume meshing was configured using ICEM software (ANSYS) to generate volume and boundary layer meshes. The boundary layers were resolved within the volume mesh to capture the boundary layer effects near the walls. The Navier−Stokes equations and continuity equations were then solved to simulate fluid flow within the IVC and bilateral common iliac veins via Fluent software (ANSYS).

To more accurately represent in vivo blood flow, blood was modelled as a homogeneous, incompressible Newtonian fluid at constant temperature with a density of 1050 kg/m^3, a viscosity coefficient of 0.0035 Pa·S, and pulsatile, laminar flow. The simulation was set up to reflect transient flow conditions, disregarding gravitational effects, and the blood vessel wall was assumed to be nonslip and rigid. The boundary conditions were defined with specific velocity inlet and pressure outlet settings[22–24].

One subject in the control group was randomly selected for ultrasound imaging of the bilateral common iliac veins. These images were utilized to extract and plot blood flow velocity curves using GetData and Prism software. The resultant curves were applied to the inlet as boundary conditions (Fig. 4). Additionally, the mean central venous pressure (1066.58 Pa) was imposed as the boundary condition at the outlet of the IVC[25].

Using a constant time step of $\Delta t = 0.005$ s, the analysis was conducted over four cardiac cycles, encompassing a total of 180 steps per cycle, ensuring transient simulation convergence. Upon convergence of the calculation results, the data from the final cycle were extracted. Postprocessing was conducted in CFD-Post software (ANSYS), followed by the identification of the time point at which the maximum flow velocity at the LCIV inlet was obtained. At this time point, numerical values and visual representations of key haemodynamic parameters, including pressure, velocity, TAWSS, and RRT, were generated. The TAWSS refers to the average shear stress on the vessel wall over the entire cardiac cycle and is calculated as follows:

$$TAWSS = \frac{1}{T}\int_0^T |WSS(s,t)| \cdot dt$$

where WSS is the instantaneous wall shear stress, T is the duration of the cardiac cycle, and S is the position of the vessel wall. The RRT is used to evaluate the residence time of particles near the vessel wall and is calculated as follows:

$$RRT = \frac{1}{(1 - 2 \cdot OSI) \cdot TAWSS}$$

where

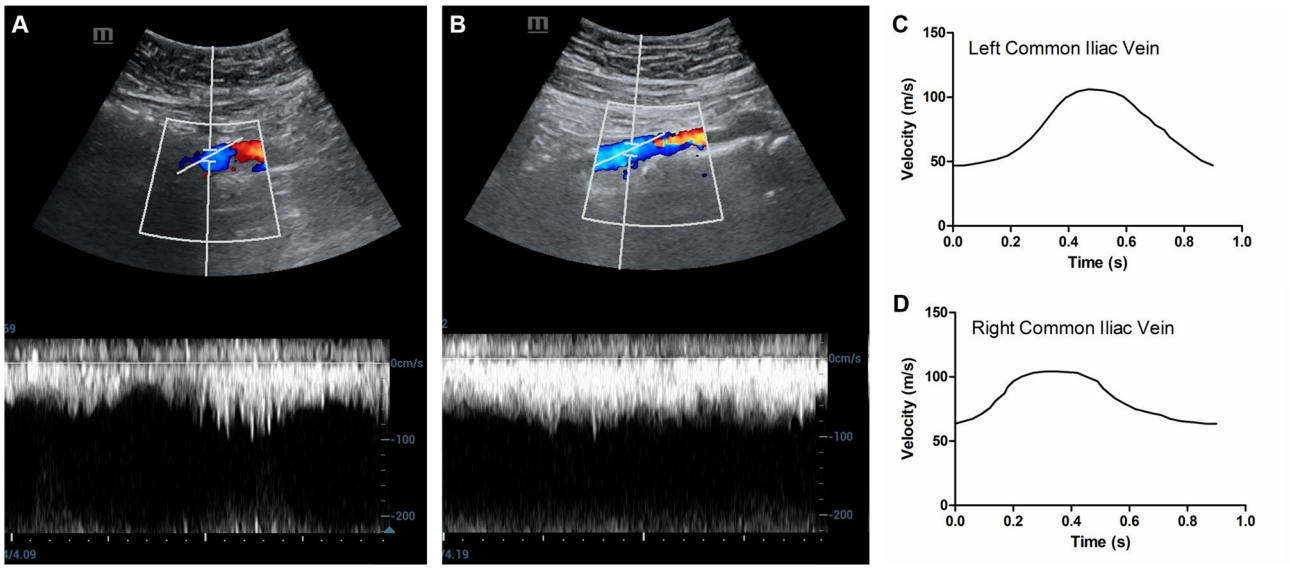

Figure 4. Blood flow velocity in the bilateral iliac veins measured by colour Doppler ultrasound. (**A**) Image showing the blood flow velocity inside the left common iliac vein (LCIV) measured via colour Doppler ultrasound; (**B**) Image showing the blood flow velocity inside the right common iliac vein (RCIV) measured via colour Doppler ultrasound; (**C**) Blood flow velocity curve of the LCIV; (**D**) Blood flow velocity curve of the RCIV.

$$OSI = 0.5\left[1 - \left(\frac{\left|\frac{1}{T}\int_0^T WSS(s,t)\cdot dt\right|}{\frac{1}{T}\int_0^T |WSS(s,t)|\cdot dt}\right)\right]$$

Morphological analysis

Morphological indicators of all subjects' vascular 3D models were measured, including the minimum cross-sectional area of the stenotic segment of the LCIV (S1), the cross-sectional area of the caudal end of the stenotic segment of the LCIV (S2), the cross-sectional area of the confluence of the bilateral common iliac veins (S3), the cross-sectional area stenosis rate of the stenotic segment of the LCIV—calculated as $\text{Cross} - \text{sectional area stenosis rate} = \left(1 - \frac{S1}{S2}\right) \times 100\%$—the bifurcation angle at the confluence of the centrelines of the bilateral common iliac veins (θ), the length of the stenotic segment of the LCIV (L1; i.e., the distance between the imprints at both ends of the LCIV observed on the 3D model), and the distance from the narrowest point of the LCIV to the confluence point of the centrelines of the bilateral common iliac veins (L2).

Statistical analysis

Statistical analysis was conducted using SPSS 23.0 (Statistical Package for Social Sciences Inc., Chicago, IL, USA). Normally distributed continuous variables are presented as the mean ± standard deviation (SD). Comparisons between two groups were conducted with the independent samples t test. Analysis involving more than two groups were conducted with repeated-measures ANOVA, followed by post hoc Bonferroni correction for multiple comparisons. The optimization function provided by the formula below was utilized to determine boundary values between groups:

$$\text{argmin}_b\left(\sqrt{\sum_{i=1}^{n}(b - x_i)^2} + \sqrt{\sum_{j=1}^{m}(b - x_j)^2}\right)$$

where b represents the decision point value, n is the number of features in the first class, m is the number of features in the second class, and x_i and x_j are the values of the features in the first and second classes, respectively. Spearman's correlation coefficients were computed to examine the relationships between haemodynamic and morphological indicators and the clinical classification. $p < 0.05$ was considered to indicate statistical significance.

Informed consent waiver statement

For this experiment, patient names and basic information have been omitted. Unique codes are assigned to represent each patient in order to ensure confidentiality and protect patient privacy. Data entry is conducted by designated personnel, and after backup of patient information, data represented by the assigned codes are provided to researchers. Therefore, except for data entry personnel, other researchers do not have access to patient information, and no information related to patient identity will be disclosed in publications, ensuring full confidentiality of patient privacy. This study is a retrospective research, making it difficult to obtain informed consent from all patients. A waiver of informed consent has been approved by Peking University Third Hospital Medical Science Research Ethics Committee, and the Ethics Review Approval Notice (Ethics Approval: 2023-675-01) has been attached as a supplementary file.

Data availability

The datasets used and/or analysed during the current study available from the corresponding author on reasonable request.

Received: 6 April 2024; Accepted: 7 August 2024
Published online: 13 August 2024

References

1. Birn, J. & Vedantham, S. May-Thurner syndrome and other obstructive iliac vein lesions: meaning, myth, and mystery. *Vasc. Med.* **20**, 74–83. https://doi.org/10.1177/1358863X14560429 (2015).
2. Raju, S. & Neglen, P. High prevalence of nonthrombotic iliac vein lesions in chronic venous disease: a permissive role in pathogenicity. *J. Vasc. Surg.* **44**, 136–144. https://doi.org/10.1016/j.jvs.2006.02.065 (2006).
3. Koksoy, C., Bahcecioglu, I. B., Cetinkaya, O. A. & Akkoca, M. Iliocaval outflow obstruction in patients with venous ulcers in a small comparison study between patients with primary varicose veins and chronic deep vein disease. *J. Vasc. Surg. Venous Lymphat. Disord.* **9**, 703–711. https://doi.org/10.1016/j.jvsv.2020.08.019 (2021).
4. Ye, K. *et al.* Long-term outcomes of stent placement for symptomatic nonthrombotic iliac vein compression lesions in chronic venous disease. *J. Vasc. Int. Radiol.: JVIR* **23**, 497–502. https://doi.org/10.1016/j.jvir.2011.12.021 (2012).
5. Zhu, R., Jin, X. & Shen, J. Efficacy analysis of endovascular therapy for nonthrombotic iliac vein compression syndrome combined with chronic venous insufficiency. *Comput. Math. Methods Med.* **2022**, 2718314. https://doi.org/10.1155/2022/2718314 (2022).
6. Ehrich, W. E. & Krumbhaar, E. B. A frequent obstructive anomaly of the mouth of the left common iliac vein. *Am. Heart J.* **26**, 18–31 (1943).
7. Lurie, F. *et al.* The 2020 update of the CEAP classification system and reporting standards. *J. Vasc. Surg. Venous Lymphat. Disord.* **8**, 342–352. https://doi.org/10.1016/j.jvsv.2019.12.075 (2020).
8. Beebe, H. G. *et al.* Classification and grading of chronic venous disease in the lower limbs. A consensus statement. *Eur. J. Vasc. Endovasc. Surg.* **12**, 487–492. https://doi.org/10.1016/s1078-5884(96)80019-0 (1996).
9. Joh, M. & Desai, K. R. Treatment of nonthrombotic iliac vein lesions. *Semin. Intervent. Radiol.* **38**, 155–159. https://doi.org/10.1055/s-0041-1727101 (2021).
10. Xue, H., Saha, S. C., Beier, S., Jepson, N. & Luo, Z. Topological optimization of auxetic coronary stents considering hemodynamics. *Front. Bioeng. Biotechnol.* **9**, 728914. https://doi.org/10.3389/fbioe.2021.728914 (2021).
11. Wang, W. *et al.* Hemodynamic analysis of sequential graft from right coronary system to left coronary system. *Biomed. Eng. Online* **15**, 132. https://doi.org/10.1186/s12938-016-0259-x (2016).
12. Ren, S. *et al.* Hemodynamic evaluation of endarterectomy and stenting treatments for carotid web. *Front. Cardiovasc. Med.* **9**, 993037. https://doi.org/10.3389/fcvm.2022.993037 (2022).
13. Salavatidezfouli, S. *et al.* Investigation of the stent induced deformation on hemodynamic of internal carotid aneurysms by computational fluid dynamics. *Sci. Rep.* **13**, 7155. https://doi.org/10.1038/s41598-023-34383-6 (2023).
14. Berger, T. & Kreibich, M. Computational fluid dynamics: a promising diagnostic tool. *Eur. J. Cardio-Thoracic Surg.: Off. J. Eur. Assoc. Cardio-Thoracic Surg.* **60**, 392. https://doi.org/10.1093/ejcts/ezab247 (2021).
15. van de Velde, L., Groot Jebbink, E., Hagmeijer, R., Versluis, M. & Reijnen, M. Computational fluid dynamics for the prediction of endograft thrombosis in the superficial femoral artery. *J. Endovasc. Ther.* **30**, 615–627. https://doi.org/10.1177/15266028221091890 (2023).
16. Feng, S., Wu, F. & Pan, X. Computational fluid dynamics as a novel method to predict haemodynamic changes and guide transcatheter edge-to-edge repair. *Eur. Heart J.* **44**, 3199. https://doi.org/10.1093/eurheartj/ehad244 (2023).
17. Kamada, H., Nakamura, M., Ota, H., Higuchi, S. & Takase, K. Blood flow analysis with computational fluid dynamics and 4D-flow MRI for vascular diseases. *J. Cardiol.* **80**, 386–396. https://doi.org/10.1016/j.jjcc.2022.05.007 (2022).
18. Wang, H. *et al.* Morphometric and hemodynamic analysis of the compressed iliac vein. *J. Endovasc. Ther.* https://doi.org/10.1177/15266028221134895 (2022).
19. Changsheng, L., Haiquan, F., Kun, W., Xiaotian, W. & Yonggang, W. Influence of the anatomical structure on the hemodynamics of iliac vein stenosis. *J. Biomech. Eng.* https://doi.org/10.1115/1.4055307 (2023).
20. Gutwein, A. & Thalhammer, C. Ultrasound-guided venous pressure measurement. *Vasa* **51**, 333–340. https://doi.org/10.1024/0301-1526/a001032 (2022).
21. Kibbe, M. R. *et al.* Iliac vein compression in an asymptomatic patient population. *J. Vasc. Surg.* **39**, 937–943. https://doi.org/10.1016/j.jvs.2003.12.032 (2004).
22. Monson, K. L., Matsumoto, M. M., Young, W. L., Manley, G. T. & Hashimoto, T. Abrupt increase in rat carotid blood flow induces rapid alteration of artery mechanical properties. *J. Mech. Behav. Biomed. Mater.* **4**, 9–15. https://doi.org/10.1016/j.jmbbm.2010.08.003 (2011).
23. Yamamoto, H. *et al.* Measurement of human blood viscosity a using Falling Needle Rheometer and the correlation to the Modified Herschel-Bulkley model equation. *Heliyon* **6**, e04792. https://doi.org/10.1016/j.heliyon.2020.e04792 (2020).
24. Zhang, T. *et al.* Application of computational fluid dynamics in hemodynamic research of aortic arch. *Zhonghua Yi Xue Za Zhi* **93**, 380–384 (2013).
25. Xing, C. Y. *et al.* New method for noninvasive quantification of central venous pressure by ultrasound. *Circ. Cardiovasc. Imaging* https://doi.org/10.1161/CIRCIMAGING.114.003085 (2015).

Acknowledgements

This research did not receive any specific grant from funding agencies in the public, commercial, or not-for-profit sectors.

Author contributions

Y.P. designed and performed experiments, analysed the data and wrote the original draft of the manuscript; QJ.L. performed experiments, analysed the data and wrote the original draft of the manuscript; X.L. designed experiments and revised the manuscript. All authors reviewed the manuscript.

Competing interests

The authors declare no competing interests.

Additional information

Supplementary Information The online version contains supplementary material available at https://doi.org/10.1038/s41598-024-69598-8.

Correspondence and requests for materials should be addressed to X.L.

Reprints and permissions information is available at www.nature.com/reprints.

Publisher's note Springer Nature remains neutral with regard to jurisdictional claims in published maps and institutional affiliations.